Electrochimica Acta 111 (2013) 455–465

Contents lists available at ScienceDirect

Electrochimica Acta

journal homepage: www.elsevier.com/locate/electacta

Ethanol electro-oxidation in an alkaline medium using Pd/C, Au/C and PdAu/C electrocatalysts prepared by electron beam irradiation

Adriana Napoleão Geraldes[a], Dionisio Furtunato da Silva[b], Eddy Segura Pino[b], Júlio César Martins da Silva[b], Rodrigo Fernando Brambilla de Souza[b], Peter Hammer[c], Estevam Vitório Spinacé[b], Almir Oliveira Neto[b], Marcelo Linardi[b], Mauro Coelho dos Santos[a,*]

[a] *Laboratório de Eletroquímica e Materiais Nanoestruturados, Centro de Ciências Naturais e Humanas, Universidade Federal do ABC, Rua Santa Adélia, 166, 09210-170 Santo André, SP, Brazil*
[b] *Instituto de Pesquisas Energéticas e Nucleares-Comissão Nacional de Energia Nuclear (IPEN-CNEN), Av. Prof. Lineu Prestes, 2242, 05508-900 São Paulo, SP, Brazil*
[c] *Universidade Estadual Paulista Júlio de Mesquita Filho, Instituto de Química de Araraquara Rua Prof. Francisco Degni, 55 Quitandinha, 14800-060 Araraquara, SP, Brazil*

ARTICLE INFO

Article history:
Received 11 June 2013
Received in revised form 2 August 2013
Accepted 3 August 2013
Available online xxx

Keywords:
Electron beam irradiation
Fuel cell
Alkaline direct ethanol fuel cell
Ethanol electro-oxidation
PdAu/C
DAAFC

ABSTRACT

Carbon-supported Pd, Au and bimetallic PdAu (Pd:Au 90:10, 50:50 and 30:70 atomic ratios) electrocatalysts were prepared using electron beam irradiation. The obtained materials were characterized by energy dispersive X-ray analysis (EDX), X-ray diffraction (XRD) and transmission electron microscopy (TEM), and their catalytic activities toward ethanol electro-oxidation were evaluated in an alkaline medium using electrochemical techniques, *in situ* attenuated total reflectance Fourier transformed infrared spectroscopy (ATR-FTIR) analysis and a single alkaline direct ethanol fuel cell (ADEFC). EDX analyses showed that the actual Pd:Au atomic ratios were very similar to the nominal ones. X-ray diffractograms of PdAu/C electrocatalysts evidenced the presence of Pd-rich (fcc) and Au-rich (fcc) phases. TEM analysis showed a homogeneous dispersion of nanoparticles on the carbon support, with an average size in the range of 3–5 nm and broad size distributions. Cyclic voltammetry (CV) and chronoamperometry (CA) experiments revealed the superior ambient activity toward ethanol electro-oxidation of PdAu/C electrocatalysts with Pd:Au ratios of 90:10 and 50:50. *In situ* ATR-FTIR spectroscopy measurements have shown that the mechanism for ethanol electro-oxidation is dependent on catalyst composition, leading to different reaction products, such as acetaldehyde and acetate, depending on the number of electrons transferred. Experiments on a single ADEFC were conducted between 50 and 90 °C, and the best performance of 44 mW cm^{-2} in 2.0 mol L^{-1} ethanol was obtained at 85 °C for the Pd:Au 90:10 catalysts. This superior performance is most likely associated with enhancement of ethanol adsorption on Pd, oxidation of the intermediates, the presence of gold oxide-hydroxyl species, low mean particle diameters and better distribution of particles on the support.

1. Introduction

Environmental problems and the increased global demand for energy have mobilized the scientific community in search of clean and renewable energy sources [1–3]. In this context, fuel cells appear to be an appropriate technology for generating electricity through the electro-oxidation of alcohols [4–8]; acid cells are the most developed variety. Methanol is the most efficient liquid fuel, and carbon-supported PtRu nanoparticles (PtRu/C electrocatalysts) are the best electrocatalysts [6]. Ethanol has also been widely studied due to its economic and environmental characteristics, with higher energy density and lower toxicity than those of methanol. However, the complete oxidation of ethanol to CO_2 is more difficult than in the case of methanol due to the requirement of C—C bond breaking and the formation of CO-like species that poison platinum catalysts [9–11]. Moreover, the slowness of anodic and cathodic reactions in acidic environments and the high price of the necessary Pt-based electrocatalysts and membranes make ethanol fuel cells an expensive technology, hindering its competitiveness [1].

The development of anion exchange membranes stimulated the research of alkaline direct ethanol fuel cells (ADEFC), in which the

* Corresponding author. Tel.: +55 11 4996 0163; fax: +55 11 4437 8400.
E-mail addresses: mauro.santos@ufabc.edu.br, drmcsa@gmail.com (M.C. dos Santos).

0013-4686/$ – see front matter © 2013 Elsevier Ltd. All rights reserved.
http://dx.doi.org/10.1016/j.electacta.2013.08.021

fuel oxidation and oxygen reduction reactions take place with faster kinetics, allowing the use of less noble metals than the expensive platinum. These membranes also offer lower permeability to fuel and allow better water management, thus simplifying the cell design, since the ionic current in the alkaline fuel cell is due to conduction of hydroxide ions. This ionic flow is in the reverse direction to that in proton conducting systems. As such, the direction of the electro-osmotic drag is reversed, reducing alcohol crossover and anodic dryness [12]. Several research groups have intensively studied the less expensive Pd-based electrocatalysts for ethanol electro-oxidation in an alkaline medium [12]. The results have shown that Pd is an active electrocatalyst toward ethanol electro-oxidation; furthermore, the combination of Pd with other metals as co-catalysts improves its activity, stability and poison tolerance [12]. Gold is generally considered a poor electrocatalyst in acidic conditions; however, its activity in alkaline conditions is slightly higher [13]. In an alkaline medium, the high activity of bimetallic electrocatalysts (PdAu/C) is related to the fact that practically no poisoning species (CO-like species) can be formed and adsorbed on gold surface. It was suggested that the easy adsorption of small organic molecules on the Pd surface and simultaneous activation of the Au surface by hydroxyl species in an alkaline medium produce a synergistic effect that improves the ethanol oxidation kinetics in PdAu binary electrocatalysts [13]. It has been shown that addition of the second metal, such as Au increases the activity of Pd-based anode catalysts for alcohol electro oxidation [11,12].

The characteristics of multi-metallic catalysts, such as activity (energy generation) and selectivity, depend on their nature, structure and composition, and can be fine-tuned during the preparation procedure [11]. Carbon-supported metal nanoparticles for fuel cell applications have been prepared by radiation-induced reduction of metal ion precursors [14]. Silva et al. prepared PtRu/C electrocatalysts for methanol electro-oxidation in acid medium using gamma and electron beam irradiation [15–17] and $PtSnO_2$/C electrocatalysts for ethanol electro-oxidation using electron beam irradiation [14]. Electron beam irradiation allowed the preparation of an active PtRu/C electrocatalyst in only a few minutes. In recent work, Silva et al. studied the activities of different electrocatalysts for alcohol electro-oxidation in an alkaline medium and reported superior performance for methanol electro-oxidation by PtAu/C electrocatalysts than by Pt/C electrocatalysts; furthermore, PtAuBi/C (50:40:10) showed the best performance in alkaline conditions [17].

The oxidation reactions of alcohols are very complex, involving several elementary steps: adsorption and alcohol dehydrogenation reactions, electron transfer and reactions with adsorbed OH groups and product desorption [18]. Therefore, active multifunctional electrocatalysts that are tolerant to poisoning CO-like species and allow the most advanced partial oxidation reaction of ethanol at lower over-potentials to enhance ethanol electro-oxidation must be developed.

In this work, Au/C, Pd/C and PdAu/C electrocatalysts with different Pd:Au atomic ratios were prepared in water/2-propanol using electron beam irradiation. The obtained materials were tested for ethanol electro-oxidation in an alkaline medium at room temperature using electrochemical techniques and in a single ADEFC, in the range of 50–90 °C. The products and intermediates formed during ethanol electro-oxidation were measured *in situ* using ATR-FTIR.

2. Experimental

Pd/C, Au/C and PdAu/C electrocatalysts (20 wt% metal loading) were prepared with different Pd:Au atomic ratios using $Pd(NO_3)_2{\cdot}2H_2O$ (Fluka) and $HAuCl_4{\cdot}3H_2O$ (Fluka) as metal sources, dissolved in 50/50 (v/v) water/2-propanol. Carbon Vulcan® XC72R, used as a support, was then dispersed in the solution using an ultrasonic bath. The resulting mixtures were submitted (at ambient conditions) under stirring to electron beam irradiation (Electron Accelerator's Dynamitron Job 188-IPEN/CNEN-SP), with a total applied dose of 288 kGy (dose rate 1.6 kGy s^{-1}, time 3 min).

Electron beam irradiation of a water solution causes the ionization and excitation of water molecules, producing the species shown in Eq. (1) [19]:

$$H_2O + \xrightarrow{\text{Electron beam}} e_{aq}^-;\ H^+,\ H^\bullet,\ H_2,\ {}^\bullet OH,\ H_2O_2 \quad (1)$$

The solvated electrons, e_{aq}^-, and $H^\bullet$ radicals are strong reducing agents and are able to reduce metal ions down to their zero-valent states (Eqs. (2) and (3)):

$$M^+ + e_{aq}{}^- \rightarrow M^0 \quad (2)$$

$$M^+ + H^\bullet \rightarrow M^0 + H^+ \quad (3)$$

However, $^\bullet OH$ radicals can oxidize ions or atoms into a higher oxidation state and thus counterbalance reduction reactions (2) and (3). Thus, an $^\bullet OH$ radical scavenger, in this case 2-propanol, is added to the above solution and reacts with these radicals, leading to the formation of radicals that are able to reduce metal ions (Eqs. (4) and (5)) [19]:

$$(CH_3)_2CHOH + {}^\bullet OH \rightarrow (CH_3)_2COH + H_2O \quad (4)$$

$$M^+ + (CH_3)_2COH \rightarrow M^0 + (CH_3)_2CO + H^+ \quad (5)$$

In this manner, the atoms produced by the reduction of metal ions progressively coalesce, leading to the formation of metal nanoparticles.

After electron beam irradiation, the mixtures were filtered, and the solids (Pd/C and PdAu/C electrocatalysts) were washed with water and dried at 70 °C for 2 h [15,16,20].

The Pd:Au atomic ratios were obtained by energy-dispersive X-ray analysis (EDX) using a Philips XL30 scanning electron microscope with a 20 keV electron beam and equipped with an EDAX DX-4 microanalyzer.

X-ray diffraction (XRD) analyses were carried out with a Miniflex II model Rigaku diffractometer using a Cu Kα source (λ = 1.54056 Å). The diffractograms were recorded at 2θ in the range 20–90° with step size of 0.05° and scan time of 2 s per step. The average crystallite size was estimated using the Scherrer equation [21].

Transmission electron microscopy (TEM) was carried out using a JEOL JEM-2100 electron microscope operated at 200 kV. The particle distribution histogram was determined by measuring 150 particles from each micrograph.

Electrochemical studies of the electrocatalysts were carried out using the thin porous coating technique [22]. A total of 20 mg of the electrocatalyst was added to a solution of 50 mL of water containing 3 drops of a 6% polytetrafluoroethylene (PTFE) suspension. The resulting mixture was treated in an ultrasound bath for 10 min, filtered and transferred to the cavity (0.30 mm deep and 0.36 cm^2 in area) of the working electrode. The reference electrode was Ag/AgCl, and the counter electrode was a platinized Pt plate.

Electrochemical measurements were carried out using a Microquimica (model MQPG01, Brazil) potentiostat/galvanostat. Cyclic voltammetry was performed using 1.0 mol L^{-1} ethanol in 1.0 mol L^{-1} KOH saturated with N_2. Chronoamperometry experiments were performed using 1.0 mol L^{-1} ethanol in 1.0 mol L^{-1} KOH at −0.40 V at room temperature.

In situ attenuated total reflectance Fourier transform infrared spectroscopy (ATR-FTIR) measurements were carried out using a Varian® 660 IR spectrometer equipped with an MCT detector

cooled with liquid N_2, a MIRacle with a Diamond/ZnSe Crystal Plate (Pike®) ATR accessory and a special cell, as presented in reference [23]. The same working electrode used in the electrochemical experiments was used in ATR-FTIR measurements. These experiments were performed at 25 °C in a 1.0 mol L^{-1} KOH solution containing 1.0 mol L^{-1} ethanol. The spectra were collected as the ratio R:R_0, where R represents a spectrum at a given potential, and R_0 is the spectrum collected at −0.70 V (in this potential, the electro oxidation of ethanol has not yet begun being still in the region of adsorption/desorption of hydrogen). Positive and negative directional bands represent gains and losses of species at the sampling potential, respectively. The spectra were computed from 96 interferograms, averaged from 2500 to 850 cm^{-1} with constant spectral resolution of 8 cm^{-1}. Initially, a reference spectrum, R_0, was measured at −0.70 V, and sample spectra were collected after applying successive potential steps from −0.85 to 0.20 V.

X-ray photoelectron spectroscopy was carried out at a pressure of less than 10^{-7} Pa using a commercial spectrometer (UNI-SPECS UHV). The Mg Kα line was used ($h\nu$ = 1253.6 eV), and the analyzer pass energy was set to 10 eV. The inelastic background of the Pd 3d, Au 4f, C 1s and O 1s electron core-level spectra was subtracted using Shirley's method. The composition of the near surface region was determined with an accuracy of about ±5% from the ratio of the relative peak areas of the corresponding elements corrected by Scofield's sensitivity factors. Multiple Voigt profiles were fit to the spectra without placing constraints. The full width at half maximum (FWHM) varied between 1.2 and 2.1 eV, and the accuracy of the peak positions was ±0.1 eV.

Membrane electrode assemblies (MEA) were prepared by hot pressing a Fumasep-FAA3-PEEK membrane (Fumasep FAA3 reinforced with PEEK and pretreated in 1.0 mol L^{-1} KOH for 24 h) between an anode of either Pd/C or PdAu/C (prepared in this work) and a cathode of 20 wt% Pd/C (prepared in this work) at 80 °C for 2 min under a pressure of 45 kgf cm^{-2}. Both electrodes used 1 mg Pd cm^{-2} catalyst loading. The ink, containing 70 wt% Pd/C or PdAu/C catalysts and 30 wt% of a 5% Nafion solution, was painted in carbon cloth. The MEA was placed between two bipolar plates and assembled in a single fuel cell with a 6 Nm torque wrench. The experiments were performed using a test bench from Electrocell Group that allows control over the fuel cell operating parameters (flow rates, humidification and temperature of the reactants and cell temperature) and performs automatic data acquisition of polarization curves and power density curves in real time. Liquid fuel alimentation made use of a Masterflex L/S Cole-Parmer peristaltic pump. The direct ethanol fuel cell performances were determined in a single cell with an area of 5 cm^2. The temperature was set between 50 and 90 °C for the fuel cell and 85 °C for the oxygen humidifier. The fuels, 1.0 and 2.0 mol L^{-1} ethanol in 1.0 and 2.0 mol L^{-1} KOH, were delivered at 1.0 mL min^{-1}, and the oxygen flow was regulated at 500 mL min^{-1}. Polarization curves were obtained by using a CDE electronic load.

3. Results and discussion

The PdAu/C electrocatalysts prepared with different Pd:Au atomic ratios using electron beam irradiation are summarized in Table 1.

For all samples, Pd:Au atomic ratios determined by EDX and XPS analysis were similar to the nominal ones.

The XRD diffractograms of Pd/C, Au/C and PdAu/C electrocatalysts, displayed in Fig. 1, show a broad peak at about 25° that was attributed to the Vulcan XC72R support. The four diffraction peaks related to the Pd/C electrocatalyst are at 2θ of approximately 40, 46, 68 and 82° and associated with the reflections of (1 1 1), (2 0 0), (2 2 0) and (3 1 1) planes, respectively, which are characteristic of the face-centered cubic (fcc) structure of Pd [19,24]. The Au/C electrocatalyst show five diffraction peaks at about 2θ = 38, 45, 65, 78 and 82°, attributed to the (1 1 1), (2 0 0), (2 2 0), (3 1 1) and (2 2 2) planes, respectively, which are characteristic of the fcc structure of Au [25]. PdAu/C (90:10) and (50:50) electrocatalysts showed separated Pd-rich (fcc) and Au-rich (fcc) phases. The PdAu/C (30:70) electrocatalyst showed only the peaks of the Au-rich (fcc) phase, indicating that, for this composition, the Pd atoms are incorporated into either an Au (fcc) phase or an amorphous phase that is not detectable by XRD [26]. In DRX analysis were not observed peaks displacements. This is suggesting that the bimetallic catalysts prepared according Spinacé et al. [20] methodology did not form alloy, contrary to what was observed by Feng et al. [27]. The authors prepared alloyed Pd_mAu nanoparticles (m refers to the atomic Pd/Au ratio) whose XRD analysis showed shifts diffraction peaks indicating the formation alloy PdAu. Applying the Scherrer equation [22], the (2 2 0) reflections of the Pd (fcc) or Au (fcc) structure were used to calculate the average crystallite sizes, which ranged between 3.0 and 5.2 nm (Table 1), in agreement to Silva et al. [14–17].

Table 1
Nominal Pd:Au atomic ratios, those obtained by EDX and XPS and crystallite sizes estimated by the Scherrer equation of PdAu/C electrocatalysts prepared using electron beam irradiation.

Pd:Au atomic ratio (nominal)	Pd:Au atomic ratio (EDX)	Pd:Au atomic ratio (XPS)	Crystallite size (nm)
PdAu 90:10	91:09	84:16	3.0
PdAu 50:50	58:42	52:48	4.5
PdAu 30:70	28:72	–	5.2

Fig. 2 shows TEM micrographs and particle size distribution histograms of Pd/C and PdAu/C (Pd:Au atomic ratios of 90:10, 50:50 and 30:70) electrocatalysts. The TEM micrographs of Pd/C and PdAu/C (Pd:Au atomic ratios of 90:10 and 50:50) electrocatalysts showed a wide distribution of nanoparticles over the carbon support, with an average particle size approximately 3.0 nm that increased slightly with Au content. The PdAu/C 30:70 electrocatalyst showed some agglomeration of the nanoparticles on the carbon support, with an average particle size approximately 5.0 nm. The histograms showed a rather broad distribution of nanoparticle sizes for all catalysts. Simões et al. [28] synthesized Pd/C, Au/C and PdAu/C electrocatalysts and observed a direct relationship between nanoparticle size and Au content. Liu et al. asserts that the activity of gold catalysts for CO oxidation is sensitive to the nature of

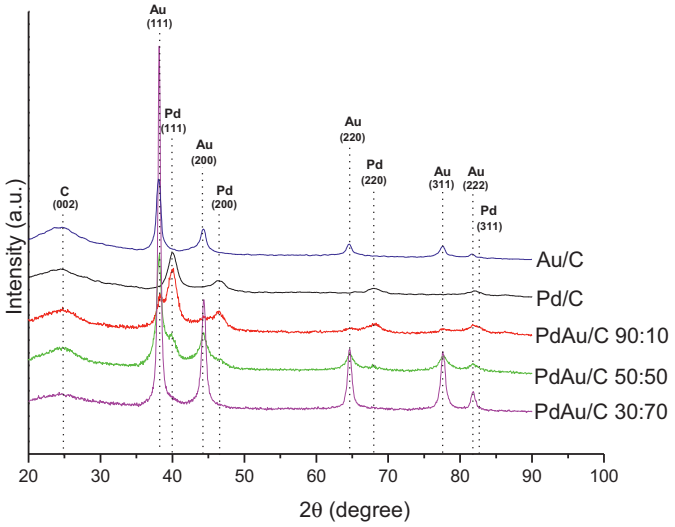

Fig. 1. X-ray diffractograms of Pd/C, Au/C and PdAu/C (90:10, 50:50 and 30:70 Pd:Au atomic ratios) prepared using electron beam irradiation.

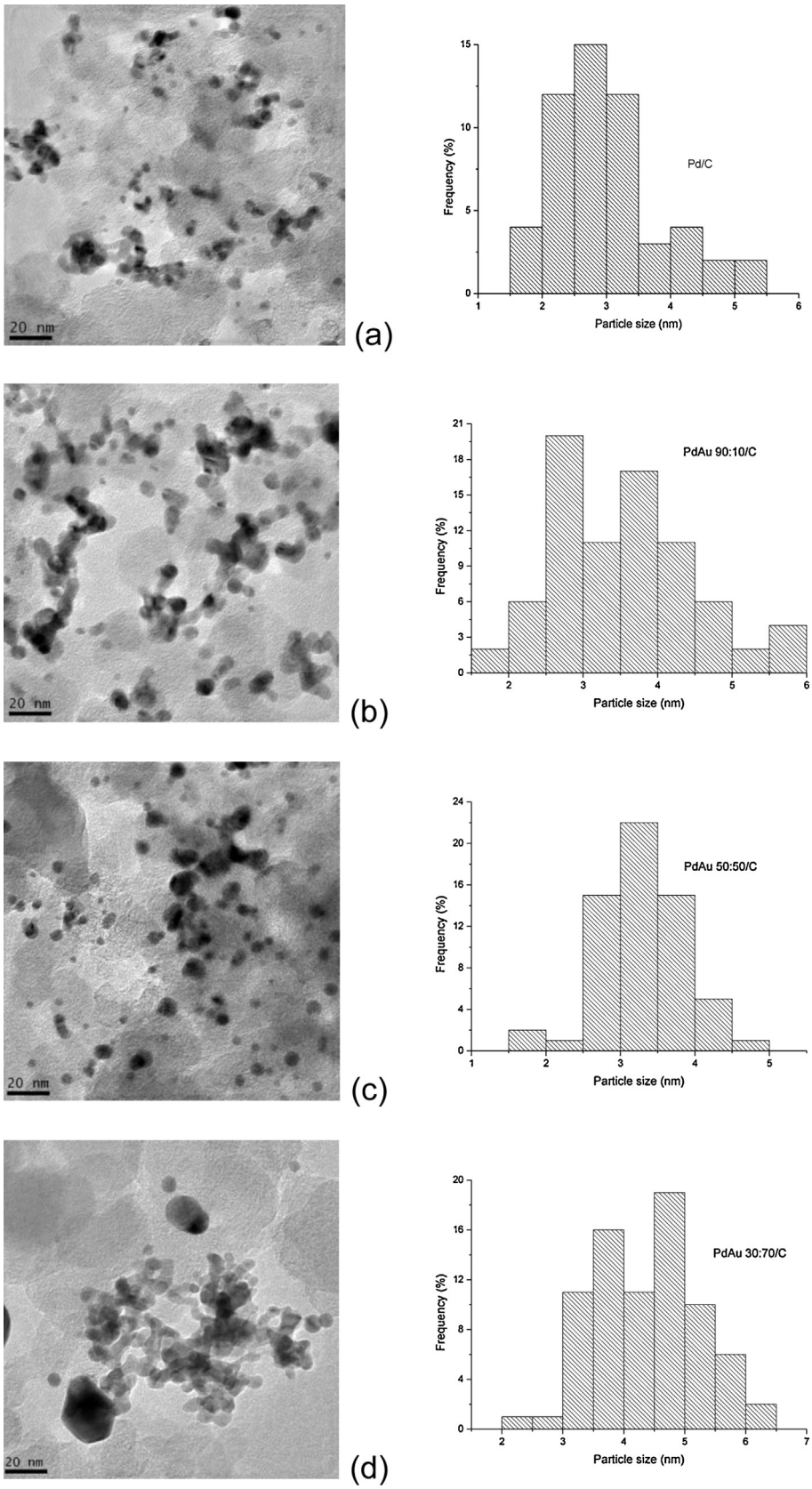

Fig. 2. TEM micrographs and particle size distribution histograms of (a) Pd/C, (b) PdAu/C (90:10), (c) PdAu/C (50:50), (d) and PtAu/C (30:70) electrocatalysts.

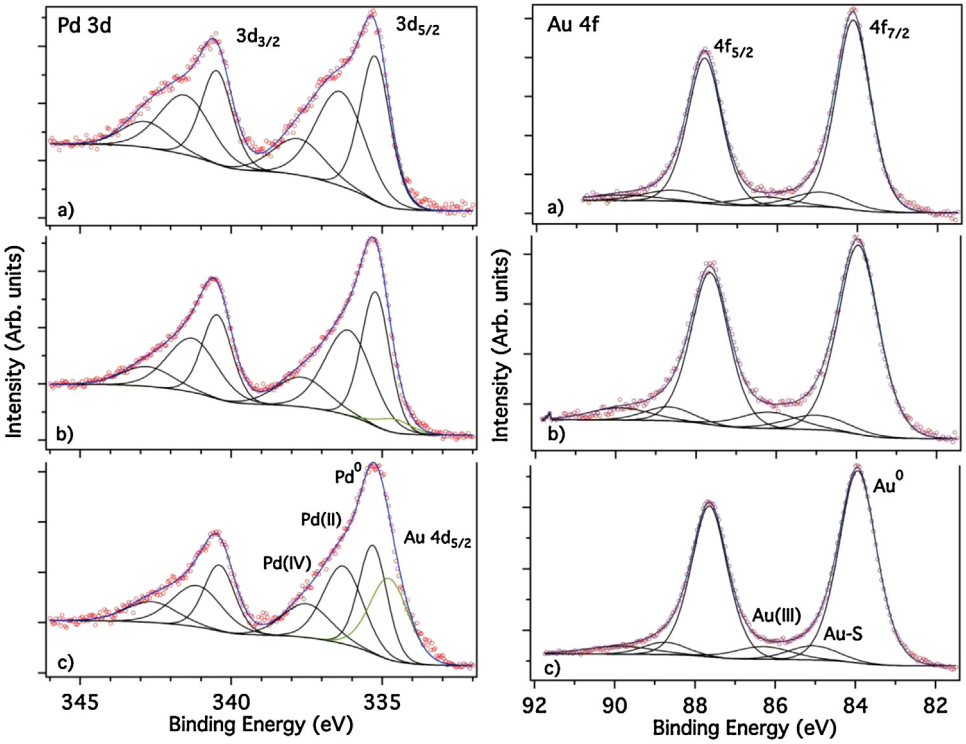

Fig. 3. Deconvoluted XPS Pd 3d and Au 4f spectra of (a) Pd/C and Au/C, (b) PdAu/C (90:10) and (c) PdAu/C (50:50) electrocatalysts.

the support, the size of the gold particles, and the properties of the gold–support interface. The low melting point of gold results in difficulty preparing gold catalysts in a highly dispersed state [29]. Also in accordance with Liu et al. the possibility of rapid Au agglomeration during catalyst preparation may be one of the main reasons that the choice of preparation method has profound effects on the catalytic activity of gold-containing materials to a much greater extent than in the cases of other noble metal catalysts.

To obtain further information on the composition and chemical states of the prepared catalysts, Pd 3d, Au 4f, C 1s and O1s core level XPS spectra were recorded. With an XPS sampling depth of approximately 4 nm and an average particle size of 3 nm, the entire volume of the catalyst was examined by the technique. The results of the quantitative analysis, shown in Table 1, indicate an equal atomic concentration of Pd and Au for the Pd:Au 50:50 sample and a slightly higher Au content than the nominal value for the Pd:Au 90:10 catalyst. This analysis supports the XRD results and confirms the formation of separate Au and Pd nanoparticles, thus excluding the possibility of a core-shell system, which would lead to the attenuation of one of the elements. In addition to elevated amounts of carbon and oxygen, traces of sulfur (0.1 at.%) and silicon (0.4 at.%) were detected, most likely on the sample surface.

Fig. 3 shows the deconvoluted high-resolution Pd 3d and Au 4f spectra of the catalysts. The Pd 3d spectrum can be fitted by three spin–orbit doublets with Pd $3d_{5/2}$ components located at 335.2, 336.3 and 337.6 eV and attributed to metallic Pd, Pd(II) and Pd(IV) phases, respectively [30]. First, the data indicate that the Pd particles consist of a metallic core embedded in a PdO sub-shell followed by a PdO_2 surface layer. Second, the constant proportion of the three phases of Pd^0:Pd(II):Pd(IV) = 1:1:0.5, detected for all samples, implies that the catalysts have very similar oxide layer profiles and that the thicknesses of the phases follow the sequence: $d(Pd^0) > d(Pd(II)) > d(Pd(IV))$. The fitted Au 4f spectra show that the gold nanoparticles are not purely metallic (main component at 84.0 eV) but possess a slightly oxidized surface, evidenced by a small component located at 86.3 eV that is indicative of an Au(III) phase, in the form of oxide or hydroxide [30]. To obtain the best fit to the data, a second spin–orbit doublet was introduced, attributed to the interaction of Au atoms with sulfur that was present in trace amounts at the particle surface. According to Mikhlin et al. [31], sulfur–gold bonds are expected at approximately 85.5 eV. In addition, the position of the S 2p peak, detected at approximately 164.0 eV (not shown), hints at the possible presence of polysulfide-like species [30].

Fig. 4 shows the assignments of the deconvoluted components of the O 1s spectra of Pd/C and Au/C electrocatalysts. These spectra

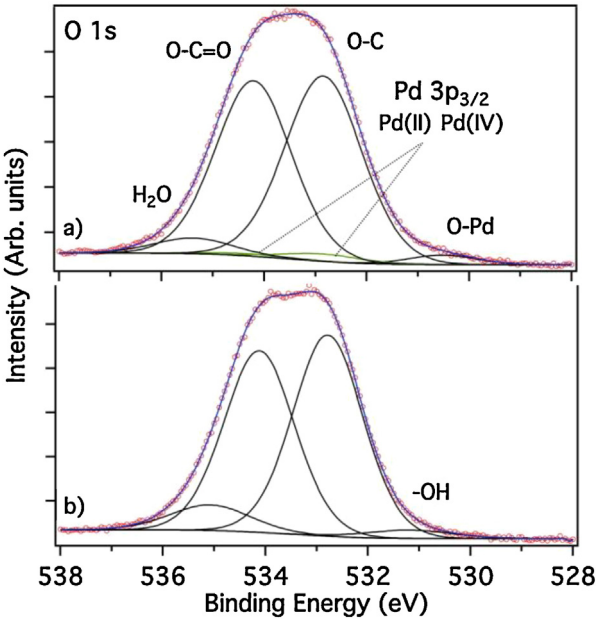

Fig. 4. Deconvoluted XPS O 1s spectra of (a) Pd/C and (b) Au/C electrocatalysts.

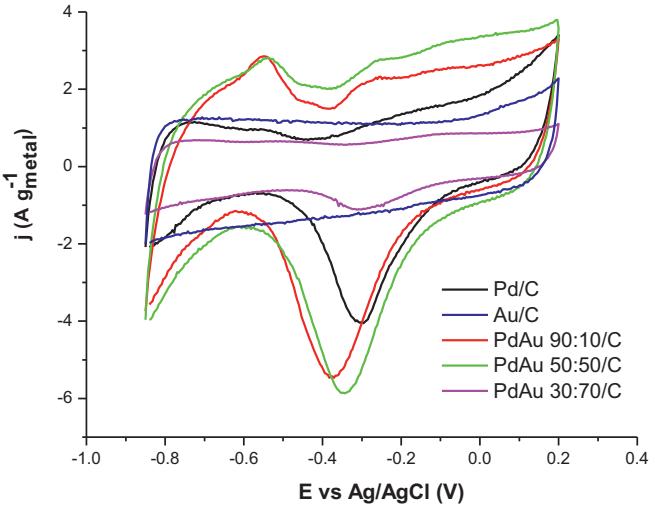

Fig. 5. Cyclic voltammograms of Pd/C, Au/C and PdAu/C electrocatalysts with atomic ratios 90:10, 50:50 and 30:70 in 1.0 mol L^{-1} KOH, measured over a potential range from −0.85 to 0.20 V *vs.* Ag/AgCl at a scan rate of 10 mV s^{-1}.

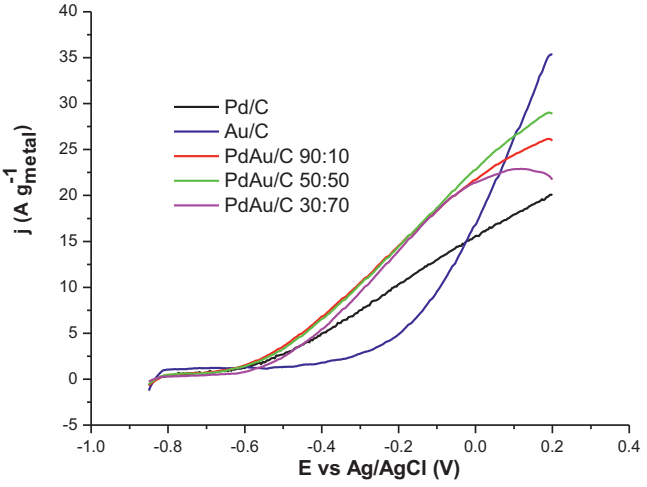

Fig. 6. Cyclic voltammograms of Pd/C, Au/C and PdAu/C (90:10, 50:50 and 30:70 Pd:Au atomic ratios) electrocatalysts in 1.0 mol L^{-1} ethanol and 1.0 mol L^{-1} KOH, measured over a potential range of −0.85 to 0.20 V *vs.* Ag/AgCl, at a scan rate of 10 mV s^{-1}.

were chosen to easily distinguish the spectral features of Pd and Au nanoparticles. The spectra are quite similar, both dominated by O—C and O—C=O groups from the Vulcan® XC72R support. The high-energy component at approximately 335.0 eV was attributed to the presence of molecular water [30], in higher abundance in the Au/C sample. The low energy component can be assigned, in the case of Pd/C, to the O^{2-} oxidation state of O—Pd bonds and, in the case of Au/C, to hydroxyl surface groups. The latter assignment supports the existence of hydroxyl species that might contribute to the catalytic activity of the Pd/Au catalysts. Finally, the C 1s peak, with a similar form for all samples (not shown), was deconvoluted into four components, with the most prominent sub-peaks at 284.6 and 285.2 eV related to the aromatic and hydrocarbon phases, respectively. The low intensity components at 286.6 and 289.2 eV represent the chemical shifts of ether/alcohol and hydroxyl groups, respectively [30].

The cyclic voltammograms (CV) of Pd/C, Au/C and PdAu/C (Pd:Au atomic ratios 90:10, 50:50 and 30:70) electrocatalysts in 1.0 mol L^{-1} KOH are shown in Fig. 5. The CV responses were normalized per gram of the metal.

CV of the Au/C electrocatalyst does not present hydrogen adsorption/desorption peaks in the positive scan (−0.85 and −0.50 V *vs.* Ag/AgCl): there is only one oxidation peak in the region between −0.1 and 0.2 V *vs.* Ag/AgCl, which is attributed to the formation of gold oxides or adsorption of OH^- species on the gold surface [32,33]. The anodic CV scan of the Pd/C electrocatalyst has one shoulder in the potential region −0.85 to −0.50 V *vs.* Ag/AgCl, associated with hydrogen adsorption/desorption processes on the Pd surface; another shoulder in the potential region −0.40 to 0.0 V and one peak in the potential region 0–0.20 V are associated with the formation of a palladium (II) oxide layer on the palladium surface [32]. Although the oxidation mechanism is not clear at present, it has been widely accepted that OH^- is first chemisorbed in the initial stage of oxide formation and then transformed into higher valence oxides at higher potentials on Pd [33]. In the negative scan, there are more pronounced reduction peaks, between −0.40 and −0.20 V *vs.* Ag/AgCl, attributed to the reduction of the Pd oxides generated during the positive scan [32]. For PdAu/C electrocatalysts (Pd:Au atomic ratios of 90:10 and 50:50), the anodic CV scan revealed that the addition of Au promotes a synergistic effect between Pd and Au that was characterized by the appearance of more pronounced peaks in the region of H_2 adsorption/desorption, suggesting that hydrogen adsorption/desorption processes on the surfaces of these electrocatalysts were favored. In addition, other more pronounced oxidation peaks appear around the same region as the previous Pd/C CV, indicating the formation of higher amounts of metallic oxides and/or greater amounts of OH^- species adsorbed on the surface of the metals. For the PdAu/C (30:70) electrocatalyst, the CV adsorption peak was similar to that of the Au/C electrocatalyst, and the reduction peak was similar to that of the Pd/C electrocatalyst; however, both peaks had small intensities. The cathodic peak at around −0.30 V in the CV of the Pd/C electrocatalysts was attributed to the reduction of the palladium oxides formed during the anodic scan. For PdAu/C (90:10) and PdAu/C (50:50) electrocatalysts, these peaks were shifted to a lower potential. The position and shape of these reduction peaks are consistent with the reduction of nanostructured Pd(II) species, either PdO or $Pd(OH)_2$ [24,34]. The shifted position of the surface oxide peak in the voltammograms, located at −0.30 and −0.38 V *vs.* Ag/AgCl for Pd/C and PdAu/C (90:10) electrocatalysts, respectively, is related to the surface composition. These results indicate that the surface is palladium rich [28]. For the PdAu/C (30:70) electrocatalyst, the peak position for surface oxide reduction was shifted to −0.33 V, which may from the influence of gold oxide reduction [35]. For the PdAu/C (50:50) the occurrence of a widening in the double layer region suggests the existence of a greater amount of adsorbed oxygen species. This widening assumes that there is higher surface area available from both species Au and Pd, at the same potential. This shows the bimetallic composition of the electrocatalysts PdAu 50:50.

Fig. 6 shows the CV obtained at room temperature for Au/C, Pd/C and PdAu/C (90:10, 50:50 and 30:70) electrocatalysts in 1.0 mol L^{-1} KOH at a scan rate of 10 mV s^{-1}, in the presence of 1.0 mol L^{-1} ethanol. The CV responses were normalized per gram of metal.

In all voltammograms, the region of hydrogen adsorption/desorption is significantly suppressed by the presence of ethanol. The voltammogram obtained from ethanol electrooxidation of Pd/C and PdAu/C (90:10, 50:50 and 30:70) electrocatalysts shows onset potential at −0.65 V *vs.* Ag/AgCl. For the Au/C electrocatalyst, the onset potential was shifted positively (−0.50 V *vs.* Ag/AgCl). The Pd/C and PdAu/C (90:10, 50:50 and 30:70) electrocatalysts showed similar performance in the region of -0.50 to 0.20 V *vs.* Ag/AgCl, while the Au/C electrocatalyst showed the lowest level of performance. Addition of the Au content to the Pd-based material could prevent the absorption of hydrogen, as reported by Hayden and coworkers [36]. These results indicate that the addition of Au to

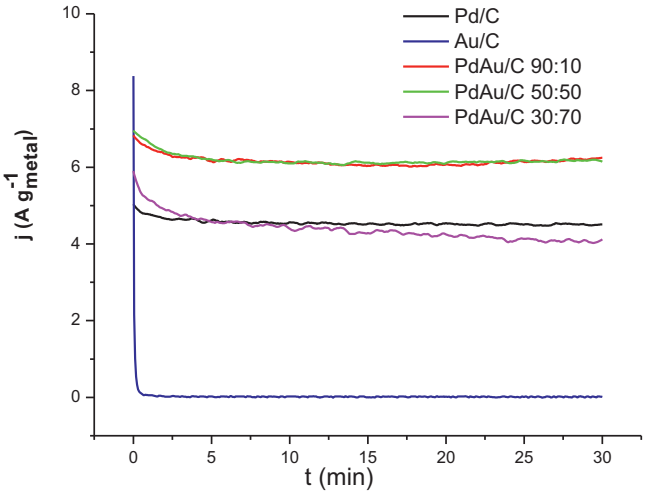

Fig. 7. Current–time curves at −0.40 V for Pd/C, Au/C and PdAu/C (90:10, 50:50 and 30:70) electrocatalysts in 1.0 mol L^{-1} ethanol in 1.0 mol L^{-1} KOH.

a Pd/C electrocatalyst improves its electrocatalytic activity over the entire potential range. The superior activity of the binary catalysts PdAu/C may be attributed to their bi-functional mechanism, superior ethanol adsorption, better dispersion and lower particle size. For a bi-functional mechanism, the OH^- species adsorbed on the second metal, near the first metal, would increase the concentration of OH_{ads} species on the electrocatalyst surface, facilitating ethanol electro-oxidation; furthermore, a wider distribution and lower particle size increase the active area for ethanol adsorption [37].

Fig. 7 shows the chronoamperometry curves obtained at room temperature for Pd/C, Au/C and PdAu/C (90:10, 50:50 and 30:70) electrocatalysts in 1.0 mol L^{-1} ethanol in 1.0 mol L^{-1} KOH, at a fixed potential of −0.40 V *vs.* Ag/AgCl for 30 min.

In each of the current–time curves, there was an initial drop in current during the first few minutes, most likely due to poisoning of the electrode by intermediates generated during ethanol electro-oxidation. PdAu/C 90:10 and 50:50 electrocatalysts showed the most superior electrocatalytic activity of all those evaluated. The PdAu/C 30:70 electrocatalyst provided an oxidation current for ethanol oxidation lower than the one for the same process using the Pd/C electrocatalyst after 5 min, while the Au/C electrocatalyst exhibited practically no activity. These results suggest that, at the investigated electrode potential, the addition of up to 50 at.% of Au to Pd/C electrocatalysts enhances their activity for ethanol electro-oxidation, yielding higher efficiency and greater tolerance to electrocatalyst poisoning.

The identification of products generated during ethanol electro-oxidation was carried out by *in situ* FTIR in the range of −0.70 to 0.20 V *vs.* Ag/AgCl using Pd/C and PdAu/C 90:10 electrocatalysts, due to their lower gold content and single fuel cell performance. FTIR spectra (Fig. 8) were recorded in 0.10 V increments, in 1.0 mol L^{-1} ethanol in 1.0 mol L^{-1} KOH aqueous solution, at room temperature.

The Pd/C and PdAu/C spectra display two intense peaks at 1553 and 1418 cm^{-1}, originating from asymmetric and symmetric C—O bond vibrations that are characteristic of the presence of acetate ions. The small peak at 926 cm^{-1} is associated with acetaldehyde C—O—O stretching vibrations [38,39]. A less intense band, associated with CO_2 symmetric stretching vibrations, is observed at 2341 cm^{-1}, suggesting the presence of a small amount of CO_2, but the intensities of this band are higher for Pd/C than for PdAu/C 90:10. These spectra also show the presence of peaks at 1047 and 1088 cm^{-1} that are associated with ethanol consumption [40]. These bands are more pronounced for PdAu/C, indicating higher ethanol consumption. Unfortunately, no band was measured in 2630 cm^{-1}, as it can be observed in Fig. 8. It is possible that this band is covered by water band, which is different from the observed by Almeida et al. [41]

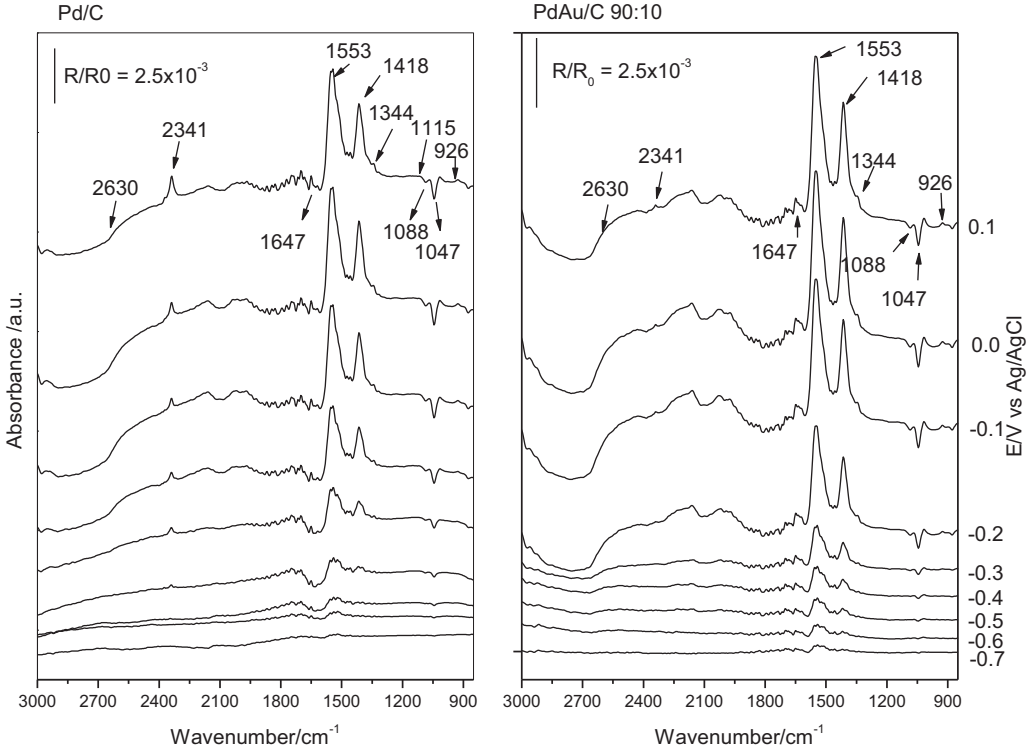

Fig. 8. *In situ* FTIR spectra of Pd/C and PdAu/C 90:10 electrocatalysts, taken in the potential range −0.70 to 0.20 V *vs.* Ag/AgCl, in 1.0 mol L^{-1} ethanol in 1.0 mol L^{-1} KOH. Each spectrum corresponds to an increase of 0.1 V compared with the spectrum below it.

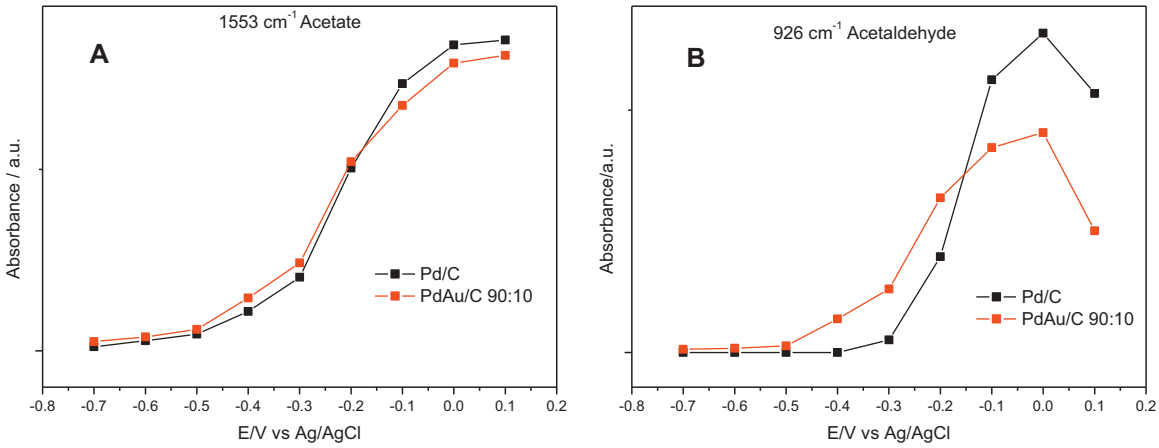

Fig. 9. Generation levels of acetate (A) and acetaldehyde (B) in the Pd/C and PdAu/C 90:10 electrocatalysts as a function of potential.

that showed a specific large band at 2630 cm^{-1} attributable to acetate.

The variations of acetate and acetaldehyde band intensity with potential were analyzed individually to compare the Pd/C and PdAu/C 90:10 electrocatalysts and the results are shown in Fig. 9.

The generation level of acetate is similar for both electrocatalysts over the entire potential range. In the case of acetaldehyde, a higher generation level was observed for the PdAu/C 90:10 electrocatalyst in the potential range between −0.20 and −0.50 V *vs.* Ag/AgCl. The PdAu/C 90:10 electrocatalyst shows very similar spectra as those of Pd/C. These results suggest that ethanol electro-oxidation on Pd/C and PdAu/C electrocatalysts occurs predominantly without C—C bond breaking, thus lowering the amounts of carbonate ion and CO_2 generated; therefore, acetate is the main product of ethanol electro-oxidation in an alkaline medium.

Although quantifying CO_2 generation was not possible, CO_2 generation requires formation of CO, which poisons the catalyst and has slower reaction kinetics. Furthermore, studies have shown that the amount of CO_2 formed is minimal, and the most

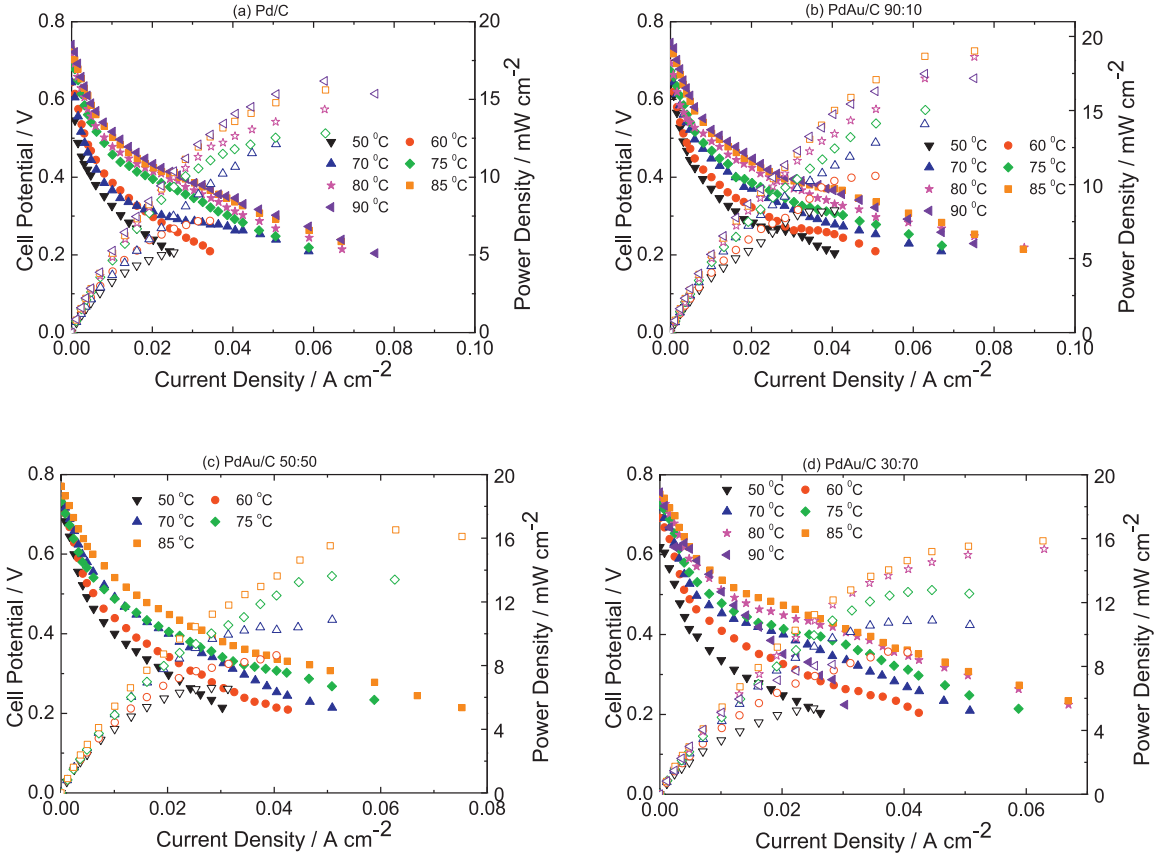

Fig. 10. Polarization and power density curves of a 5 cm^2 ADEFC operating from 50 to 90 °C and using a (a) Pd/C, PdAu/C (b) 90:10, (c) 50:50 or (d) 30:70 anodic electrocatalyst and a Pd/C cathodic electrocatalyst fed with 1.0 mol L^{-1} ethanol in 1.0 mol L^{-1} KOH solution; the anodic and cathodic catalyst loading levels were both 1 mg Pd cm^{-2}, and the ADEFC used a Fumasep-FAA3-PEEK membrane and oxygen humidifier temperature of 85 °C.

Table 2
Values of the cell open circuit voltage (OCV) and maximum power density achieved at 85 °C, with fuel flow of 1.0 mL min^{-1} and oxygen flow of 500 mL min^{-1} (both at atmospheric pressure). Fuel was fed with 1.0 and 2.0 mol L^{-1} ethanol in 1.0 and 2.0 mol L^{-1} KOH solutions using Pd/C and PdAu/C (Pd:Au of 90:10, 50:50 and 30:70) electrocatalysts.

Electrocatalyst	Ethanol 1.0 mol L^{-1}		Ethanol 2.0 mol L^{-1}	
	P_{max}/mW cm^{-2}	OCV/mV	P_{max}/mW cm^{-2}	OCV/mV
Pd/C	16	727	25	717
PdAu/C 90:10	19	732	44	751
PdAu/C 50:50	17	771	32	795
PdAu/C 30:70	16	751	30	775

active electrocatalysts are less selective to CO_2 and preferentially generate acetate and acetaldehyde [39].

Fig. 10 displays the single fuel cell performances in the temperature range 50–90 °C of Pd/C and PdAu/C (90:10, 50:50 and 30:70) electrocatalysts fed with 1.0 mol L^{-1} ethanol in 1.0 mol L^{-1} KOH.

The performance of each electrode was significantly improved as temperature increased, indicating that the ethanol electrooxidation processes are thermally activated. The highest current and power densities were obtained at approximately 85 °C for 1.0 mol L^{-1} ethanol in 1.0 mol L^{-1} KOH. Above this temperature, water management and membrane dryness began to interfere with electrode performance, most likely due to an increase in cell resistance. At 85 °C, all electrodes fed with 1 mol L^{-1} ethanol in 1 mol L^{-1} KOH had similar maximum power densities (see Table 2).

Fig. 11 shows the single fuel cell performances between 50 and 90 °C of Pd/C and PdAu/C (90:10, 50:50 and 30:70) electrocatalysts fed with 2.0 mol L^{-1} ethanol in 2.0 mol L^{-1} KOH.

As the polarization and power density curves indicate, the largest power density was detected at 85 °C for both ethanol concentrations. In addition, for both concentrations, when the operation temperature was increased, the decay of the *I–V* curve is less pronounced in the electrochemical kinetics-controlled low current density region (0.02 A cm^{-2} for 1.0 mol L^{-1} ethanol; 0.03 A cm^{-2} for 2.0 mol L^{-1} ethanol), indicating that the ethanol oxidation kinetics was greatly enhanced at higher temperatures. In the ohmic drop region, associated with electrical resistance, the plot slope decreases with increasing temperature for both ethanol concentrations. Furthermore, both concentrations reach a maximum current without exponential decay associated with mass transport limitations, indicating that the electrode kinetics may be improved without changing any physical characteristics, such as porosity and fuel supply; in other words, all losses are associated with the kinetics and resistivity of the electrodes. Above 90 °C, a decrease in cell performance was observed. These results indicate that better reactant diffusion and higher electrode kinetics may be achieved at higher temperatures. Increases of both OCV and power density increase the fuel cell concentration and temperature. The main results of the single ADEFC experiments are summarized in Table 2.

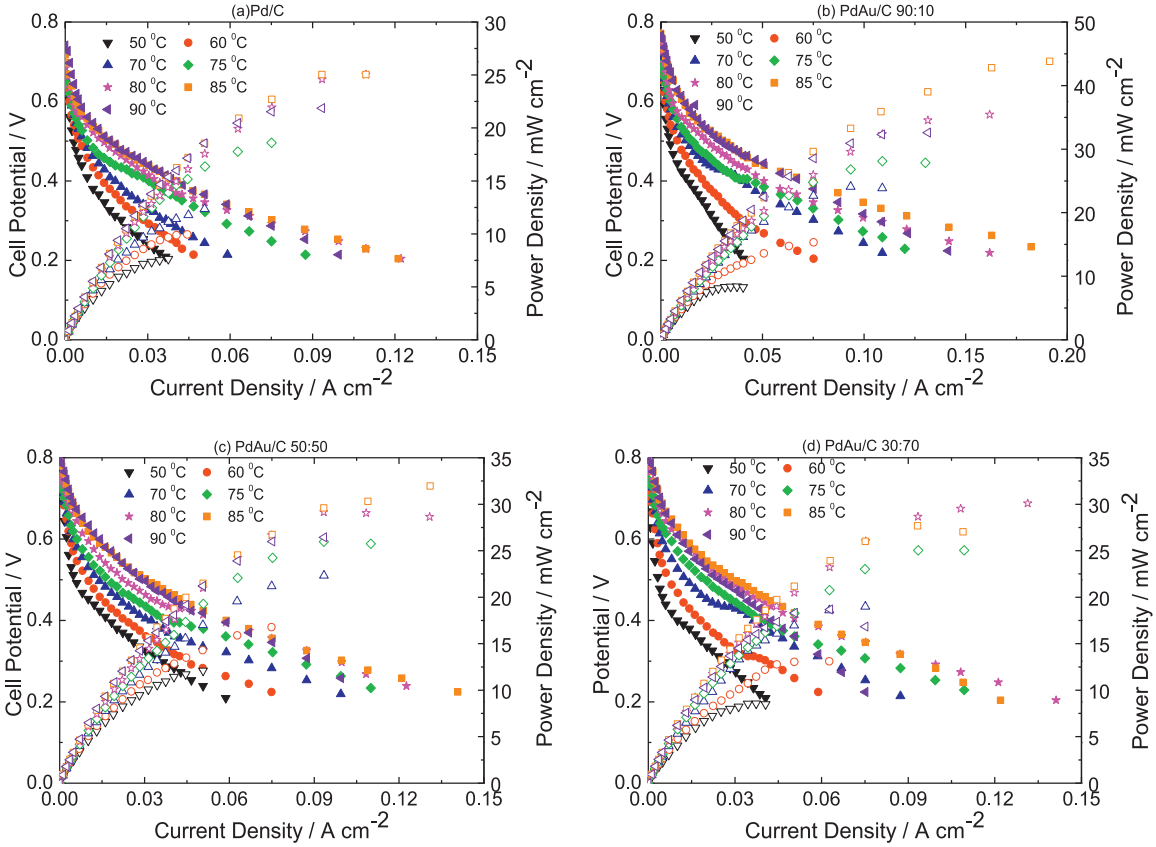

Fig. 11. Polarization and power density curves of a 5 cm^2 ADEFC operating from 50 to 90 °C and using a (a) Pd/C, PdAu/C (b) 90:10, (c) 50:50 or (d) 30:70 anodic electrocatalyst and a Pd/C cathodic electrocatalyst fed with 2.0 mol L^{-1} ethanol in 2.0 mol L^{-1} KOH solution; the anodic and cathodic catalyst loading levels were both 1 mg Pd cm^{-2}, and the ADEFC used a Fumasep-FAA3-PEEK membrane and oxygen humidifier temperature of 85 °C.

The values in Table 2 show that the highest power density generated at 85 °C was 44 mW cm^{-2}, obtained with the PdAu/C 90:10 MEA, followed by 32 mW cm^{-2} with the PdAu/C 50:50 MEA, both fed with 2.0 mol L^{-1} ethanol, indicating that 85 °C is the best operating temperature of MEAs based on palladium. The maximum power density using the PdAu/C 90:10 electrocatalyst (44 mW cm^{-2}) was higher than that using the Pd/C electrocatalyst (26 mW cm^{-2}). The PdAu/C 30:70 electrocatalyst shows lower power density throughout the potential range examined. Table 2 also shows that at 85 °C, Pd/C and PdAu/C electrocatalysts generate similar power densities for 1.0 mol L^{-1} ethanol electro-oxidation, regardless of the Pd:Au atomic ratio. At the same temperature, 2.0 mol L^{-1} ethanol electro-oxidation nearly doubled its power density, and PdAu/C binary electrocatalysts generated higher power densities than did Pd/C electrocatalysts. The single-cell tests showed that the addition of up to 90 at.% of Au to the PdAu/C catalyst enhances its activity for the electro-oxidation of ethanol, in agreement with cyclic voltammetry and chronoamperometry results.

Santasalo-Aarnio et al. [42] studied the anion exchange membrane Fumasep® FAA-2. Fuel cell experiments in 1 mol L^{-1} methanol with FAA-2 resulted in OCV of 0.58 V and a maximum power density of 0.32 mW cm^{-2}; even higher current densities were obtained with highly concentrated fuels. Simões et al. [28] investigated the oxidation of ethanol in PdAu/C electrocatalysts and proposed that the presence of a co-catalyst promotes changes in the mechanism of ethanol electro-oxidation, leading to an activity increase. Mougenot et al. [43] studied PdAu (70:30) catalysts and alternately sputtered PdAuPd (35:30:35) and AuPdAu (15:70:15) materials prepared by plasma deposition of Au and Pd on a carbon diffusion layer. They concluded that the modification of the palladium surface by gold atoms leads to an increase in the catalytic activity toward ethanol electro-oxidation. The PdAu surface alloy composition had no significant effect on the catalytic activity; however, the presence of non-alloyed gold sites on the surface led to the enhancement of catalytic activity. The mechanism seems to involve ethanol adsorption on the palladium surface and hydroxyl formation on the gold surface, leading to catalytic activity enhancement through the bi-functional mechanism. Ilie et al. [44] tested the commercial anionic membrane FUMAPEM® FAA from Fumatech. The tests were performed in a 5 cm^2 cell with identical anode and cathode (Pt (40 wt%)/C and 2 mg Pt cm^{-2} deposited on a diffusion layer carbon cloth with PTFE (15 wt%)/C). The fuel composition was 1.0 mol L^{-1} ethanol in 4.0 mol L^{-1} NaOH, and oxygen was used as an oxidant. The power densities achieved with the Fumatech membrane were 13.5 mW cm^{-2} at 60 °C and 7.8 mW cm^{-2} at 25 °C.

Reactions in an ADEFC, with ethanol fuel in KOH, presumably occur with higher kinetics than those in an acid fuel cell. Under these circumstances, the possibility of either decreasing Pt loading or even using non-platinum-based catalysts may be considered. Several reports showed that some Pt-based and Pd-based catalysts display high catalytic activity toward the electro-oxidation of alcohols or polyols in an alkaline medium [24,37,44,45]. Moreover, Pd-based bimetallic electrocatalysts seem to be more stable with respect to degradation than pure Pd on carbon black [44,46,47].

4. Conclusions

The obtained results showed that the addition of Au to Pd electrocatalysts prepared by electron beam irradiation leads to the formation of Pd-rich (fcc) and Au-rich (fcc) phases. Electrochemical experiments at room temperature revealed that the addition of 50–90 at.% of Au to Pd leads to more active electrocatalysts for ethanol electro-oxidation. Chronoamperometric experiments showed that PdAu/C (90:10 and 50:50 Pd:Au atomic ratios) electrocatalysts present similar current densities that are higher than that of Pd/C for 1.0 mol L^{-1} ethanol electro-oxidation. *In situ* ATR-FTIR experiments identified acetate and acetaldehyde as the principal products of ethanol electro-oxidation using Pd/C and PdAu/C electrocatalysts. In single fuel cell tests, the optimum operating temperature was 85 °C for ethanol electro-oxidation in Pd-based electrocatalysts. At 85 °C, the performance of the PdAu/C (90:10 atomic ratio) electrocatalyst in 2.0 mol L^{-1} ethanol solution showed the highest power density (44 mW cm^{-2}). The promoting effect of the second metal has been explained by several intrinsic features: (i) a bi-functional mechanism, in which Au adsorbs and increases the concentration of OH^- species in proximity to Pd, favoring the oxidation of ethanol/intermediary adsorbed to the Pd surface, (ii) quite low particle diameter, (iii) increased surface area, (iv) better distribution on the support, (v) low levels of poisoning by adsorbed CO, (vi) increased kinetics for acetaldehyde production.

Acknowledgments

The authors thank FAPESP (10/16511-6), CNPq, CAPES and INCT Instituto Nacional de Ciência e Tecnologia (INCT) de Energia e Meio Ambiente (Process Number 573.783/2008-0) for financial support and CTR and CCTM from IPEN/CNEN-SP for electron beam irradiations and TEM measurements.

References

[1] G. Hoogers, Fuel Cell Technology Handbook, CRC Press, 2002.
[2] M. Carmo, G. Doubek, R.C. Sekol, M. Linardi, A.D. Taylor, Development and electrochemical studies of membrane electrode assemblies for polymer electrolyte alkaline fuel cells using FAA membrane and ionomer, J. Power Source 230 (2013) 169.
[3] A. Brouzgou, S.Q. Song, P. Tsiakaras, Low and non-platinum electrocatalysts for PEMFCs: current status, challenges and prospects, Appl. Catal. B: Environ. 127 (2012) 371.
[4] S.Y. Shen, T.S. Zhao, J.B. Xu, Y.S. Li, Synthesis of PdNi catalysts for the oxidation of ethanol in alkaline direct ethanol fuel cells, J. Power Source 195 (2010) 1001.
[5] A.O. Neto, R.R. Dias, M.M. Tusi, M. Linardi, E.V. Spinacé, Electro-oxidation of methanol and ethanol using PtRu/C PtSn/C and PtSnRu/C electrocatalysts prepared by an alcohol-reduction process, J. Power Source 166 (2007) 87.
[6] H. Liu, C. Song, L. Zhang, J. Zhang, H. Wang, D.P. Wilkinson, A review of anode catalysis in the direct methanol fuel cell, J. Power Source 155 (2006) 95.
[7] A. Brouzgou, A. Podias, P. Tsiakaras, PEMFCS and AEMFCs directly fed with ethanol: a current status comparative review, J. Appl. Electrochem. 43 (2013) 119.
[8] L.V. Kumar, S.A. Ntim, O.S. Khow, C. Janardhana, V. Lakshminarayanan, S. Mitra, Electro-catalytic activity of multiwall carbon nanotube-metal (Pt or Pd) nanohybrid materials synthesized using microwave-induced reactions and their possible use in fuel cells, Electrochim. Acta 83 (2012) 40.
[9] W.J. Zhou, W.Z. Li, S.Q. Song, Z.H. Zhou, L.H. Jiang, G.Q. Sun, Q. Xin, K. Poulianitis, S. Kontou, P. Tsiakaras, Bi- and tri-metallic Pt-based anode catalysts for direct ethanol fuel cells, J. Power Source 131 (2004) 217.
[10] S. Rousseau, C. Coutanceau, C. Lamy, J.M. Léger, Direct ethanol fuel cell (DEFC): electrical performances and reaction products distribution under operating conditions with different platinum-based anodes, J. Power Source 158 (2006) 18.
[11] E. Antolini, Catalysts for direct ethanol fuel cells, J. Power Source 170 (2007) 1.
[12] E.H. Yu, U. Krewer, K. Scott, Principles materials aspects of direct alkaline alcohol fuel cells, Energies 3 (2010) 1499.
[13] G. Tremiliosi-Filho, E.R. Gonzalez, A.J. Motheo, E.M. Belgsir, J.M. Léger, C. Lamy, Electro-oxidation of ethanol on gold: analysis of the reaction products and mechanism, J. Electroanal. Chem. 444 (1998) 31.
[14] D.F. Silva, A.N. Geraldes, A.O. Neto, E.S. Pino, M. Linardi, E.V. Spinacé, W.A.A. Macedo, J.D. Ardisson, Preparation of $PtSnO_2$/C electrocatalysts using electron beam irradiation, Mater. Sci. Eng. B 175 (2010) 261.
[15] D.F. Silva, A.O. Neto, E.S. Pino, M. Linardi, E.V. Spinacé, PtRu/C electrocatalysts prepared using γ-irradiation, J. Power Source 170 (2007) 303.
[16] D.F. Silva, A.O. Neto, E.S. Pino, M. Brandalise, M. Linardi, E.V. Spinacé, PtRu/C electrocatalysts prepared using electron beam irradiation, Materials Research 10 (2007) 367.
[17] D.F. Silva, A.N. Geraldes, E.Z. Cardoso, M.M. Tusi, M. Linardi, E.V. Spinacé, A.O. Neto, Preparation of PtAu/C and PtAuBi/C electrocatalysts using electron beam irradiation for methanol and ethanol electro-oxidation in alkaline medium, Int. J. Electrochem. Sci. 6 (2011) 3594.
[18] F. Vigier, S. Rousseau, C. Coutanceau, J.M. Leger, C. Lamy, Electrocatalysis for the direct alcohol fuel cell, Top. Catal. 40 (2006) 111.
[19] J. Belloni, M. Mostafavi, H. Remita, J.L. Marignier, M.O. Delcourt, Radiation-induced synthesis of mono- and multi-metallic clusters and nanocolloids, New J. Chem. 22 (1998) 1239.

[20] E.V. Spinacé, A.O. Neto, M. Linardi, D.F. Silva, E.S. Pino, V.A. Cruz, Patent BR200505416-A.
[21] V. Radmilovic, H.A. Gasteiger, P.N. Ross, Structure and chemical composition of a supported Pt–Ru electrocatalyst for methanol oxidation, J. Catal. 154 (1995) 98.
[22] A.O. Neto, M.J. Giz, J. Perez, E.A. Ticianelli, E.R. Gonzalez, The electro-oxidation of ethanol on Pt–Ru and Pt–Mo particles supported on high-surface-area carbon, J. Electrochem. Soc. 149 (2002) A272.
[23] J.C.M. Silva, L.S. Parreira, R.F.B. De Souza, M.L. Calegaro, E.V. Spinacé, A.O. Neto, M.C. Santos, PtSn/C alloyed and non-alloyed materials: differences in the ethanol electro-oxidation reaction pathways, Appl. Catal. B: Environ. 110 (2011) 141.
[24] V. Bambagioni, C. Bianchini, A. Marchionni, J. Fillipi, F. Vizza, J. Teddy, P. Serp, M. Zhiani, Pd and Pt–Ru anode electrocatalysts supported on multi-walled carbon nanotubes and their use in passive and active direct alcohol fuel cells with an anion-exchange membrane (alcohol = methanol, ethanol, glycerol), J. Power Source 190 (2009) 241.
[25] A.F. Lee, C.J. Baddeley, C. Hardacre, R.M. Ormerod, R.M. Lambert, Structural and catalytic properties of novel Au/Pd bimetallic colloid particles: EXAFS, XRD, and acetylene coupling, J. Phys. Chem. 99 (1995) 6096.
[26] S.L. Medway, C.A. Lucas, A. Kowal, R.J. Nichols, D. Johnson, In situ studies of the oxidation of nickel electrodes in alkaline solution, J. Electroanal. Chem. 587 (2006) 172.
[27] Y. Feng, Z. Liu, Y. Xu, P. Wang, W. Wang, D. Kong, Highly active PdAu alloy catalysts for ethanol electro-oxidation, J. Power Source 232 (2013) 99.
[28] M. Simões, S. Baranton, C. Coutanceau, Electro-oxidation of glycerol at Pd based nano-catalysts for an application in alkaline fuel cells for chemicals and energy cogeneration, Appl. Catal. B: Environ. 93 (2010) 354.
[29] H. Liu, A.I. Kozlov, A.P. Kozlova, T. Shido, K. Asakura, Y. Iwasawa, Active oxygen species and mechanism for low-temperature CO oxidation reaction on a TiO_2-supported au catalyst prepared from $Au(PPh_3)(NO_3)$ and As-precipitated titanium hydroxide, J. Catal. 185 (1999) 252.
[30] NIST X-ray Photoelectron Spectroscopy Database, AV. Naumkin, A. Kraut-Vass, S.W. Gaarenstroom, C.J. Powell, NIST Standard Reference Database 20, v.4.1: http://srdata.nist.gov/XPS
[31] Y. Mikhlin, M. Likhatski, Y. Tomashevich, A. Romanchenko, S. Erenburg, S. Trubina, XAS and XPS examination of the Au–S nanostructures produced via the reduction of aqueous gold(III) by sulfide ions, J. Electron Spectrosc. Rel. Phenom. 177 (2010) 24.
[32] J.B. Xu, T.S. Zhao, Y.S. Li, W.W. Yang, Synthesis and characterization of the Au-modified Pd cathode catalyst for alkaline direct ethanol fuel cells, Int. J. Hydrogen Energy 35 (2010) 9693.
[33] Z.X. Liang, T.S. Zhao, J.B. Xu, Mechanism study of the ethanol oxidation reaction on palladium in alkaline media, Electrochim. Acta 54 (2009) 2203.
[34] C.C. Hu, T.C. Wen, Voltammetric investigation of palladium oxides—I: their formation/reduction in NaOH, Electrochim. Acta 40 (1995) 495.
[35] M. Simões, S. Baranton, C. Coutanceau, Electrooxidation of sodium borohydride at Pd, Au, and Pd_xAu_{1-x} carbon-supported nanocatalysts, J. Phys. Chem. C 113 (2009) 13369.
[36] F.A. Al-Odail, A. Anastasopoulos, B.E. Hayden, The hydrogen evolution reaction and hydrogen oxidation reaction on thin film PdAu alloy surfaces, Phys. Chem. Chem. Phys. 12 (2010) 11398.
[37] C. Bianchini, P.K. Shen, Palladium-based electrocatalysts for alcohol oxidation in half cells and in direct alcohol fuel cells, Chem. Rev. 109 (2009) 4183.
[38] T. Yajima, N. Wakabayashi, H. Uchida, M. Watanabe, Adsorbed water for the electro-oxidation of methanol at Pt–Ru alloy, Chem. Commun. 7 (2003) 828.
[39] X. Fang, L. Wang, P.K. Shen, G. Cui, C. Bianchini, An in situ Fourier transform infrared spectroelectrochemical study on ethanol electrooxidation on Pd in alkaline solution, J. Power Source 195 (2010) 1375.
[40] M.M.O. Thotiyl, T.R. Kumar, S. Sampath, Pd supported on titanium nitride for efficient ethanol oxidation, J. Phys. Chem. C 114 (2010) 17934.
[41] T.S. Almeida, L.M. Palma, P.H. Leonello, C. Morais, K.B. Kokoh, A.R. Andrade, An optimization study of PtSn/C catalysts applied to direct ethanol fuel cell: effect of the preparation method on the electrocatalytic activity of the catalysts, J. Power Source 215 (2012) 53.
[42] A. Santasalo-Aarnio, S. Hietalab, T. Rauhalaa, T. Kallio, In and ex situ characterization of an anion-exchange membrane for alkaline direct methanol fuel cell (ADMFC), J. Power Source 196 (2011) 6153.
[43] M. Mougenot, A. Caillard, M. Simões, S. Baranton, C. Coutanceau, P. Brault, PdAu/C catalysts prepared by plasma sputtering for the electro-oxidation of glycerol, Appl. Catal. B: Environ. 107 (2011) 372.
[44] A. Ilie, M. Simões, S. Baranton, C. Coutanceau, S. Martemianov, Influence of operational parameters and of catalytic materials on electrical performance of direct glycerol solid alkaline membrane fuel cells, J. Power Source 196 (2011) 4965.
[45] P.K. Shen, C. Xu, Alcohol oxidation on nanocrystalline oxide Pd/C promoted electrocatalysts, Electrochem. Commun. 8 (2006) 184.
[46] M.R. Tarasevich, V.A. Bogdanovskaya, L.N. Kuznetsova, A.D. Modestov, B.N. Efremov, A.E. Chalykh, Y.G. Chirkov, N.A. Kapustina, M.R. Ehrenburg, Development of platinum-free catalyst and catalyst with low platinum content for cathodic oxygen reduction in acidic electrolytes, J. Appl. Electrochem. 37 (2007) 1503.
[47] M.R. Tarasevich, G.V. Zhutaeva, V.A. Bogdanovskaya, M.V. Radina, M.R. Ehrenburg, A.E. Chalykh, Oxygen kinetics and mechanism at electrocatalysts on the base of palladium–iron system, Electrochim. Acta 52 (2007) 5108.